X-Disciplinarity
DOI: https://doi.org/10.63174/xdi.UVNB2355
Review

Analysis of Methods to Break Through the Free Spectral Range Limitation

https://doi.org/10.63174/xdi.UVNB2355
Volume 2 Issue 4
Received: 2 Jul 2026
Accepted: 16 Jul 2026
Published: 17 Jul 2026
Open Access

Hao Mi[1], Zhen Zhang[1], Ruiting Li[1], Faqian Liu[1], Mengchao Gao[1], Hongdi Wang[1], Qicheng Gai[1], Duo Chen[1*]

Abstract: The Free Spectral Range (FSR) is a key intrinsic parameter of interferometric and resonant photonic devices, and it has a trade-off relationship with the device sensitivity and dynamic range of measurement. This trade-off has become a critical bottleneck that limit to improve the performance of fiber optic sensing, integrated photonic filtering, and microcavity optoelectronic devices. Therefore, it has becomean an important research direction in photonic sensing and integrated photonics to break through the FSR limitation while maintaining both high sensitivity and large measurement range. This paper systematically reviews four major technical routes: demodulation algorithms, deep learning approaches, structural design, and material selection and properties. For each route, the implementation principles, research progress, and performance advantages of representative schemes are discussed. Finally, the current challenges are summarized, and the development trend toward multi-technology integration is envisioned.

1. Introduction

Sensing technology has been widely used in our daily lives. Due to inherent advantages such as resistance to electromagnetic interference, high sensitivity, long-distance distributed measurement, and intrinsic safety, optical fiber sensing technology has been applied in industrial monitoring, smart cities, biomedical fields, and more [1]-[5]. FSR is an inherent property of optical resonators, interferometers, and similar devices. Essentially, FSR represents the periodic wavelength of optical resonance, defined as the wavelength difference between two adjacent resonant peaks (or interference dips) in an optical resonant interference system. This range determines the unambiguous measurement range of resonant optical devices. Besides, overcoming the limitations of FSR is crucial to address the trade-off between sensitivity and measurement range.

Recent studies illustrate several routes for overcoming the limitation of the FSR. Hu et al. [6] used LSTM-assisted processing of the full MZI interference spectrum to analyze features beyond peak/valley positions, including spectral shape, intensity, and phase. Thereby extending the measurable refractive-index range to three FSRs while maintaining high sensitivity. Wei et al. [7] proposed stabilized triple-phase demodulation based on a 3×3 coupler, and Guo et al. [8] employed a three-wavelength self-compensating algorithm for dynamic F-P pressure sensing, showing how phase demodulation can reduce dependence on full-spectrum tracking. In structural approaches, Cuando-Espitia et al. [23] used the Vernier effect generated by highly coupled multicore fibers to improve temperature sensitivity, while Lee et al. [26] used refractive-index-selected liquid filling in a hollow-core fiber Mach-Zehnder interferometer to obtain an ultrabroad single-wavelength dip. For microresonators, Crespo-Ballesteros and Sumetsky [43] achieved ultra-precise, sub-picometer FSR tuning in a parabolic microresonator induced by optical-fiber bending. These studies indicate that algorithmic demodulation, deep learning, structural design, and material or refractive-index engineering can contribute to overcoming the FSR bottleneck. This paper discusses the core methods for overcoming the limitations of the FSR, compares representative approaches, and analyzes their performance by examining the experimental processes, procedural analyses, and experimental results of each method. The review is organized in four routes: traditional demodulation algorithms, deep learning approaches, structural design, and material selection/properties. Based on this structure, the current challenges and future research directions to overcome the bottleneck are summarized.

2. The Inherent Contradiction and Bottleneck of the Free Spectral Range

The inherent contradiction of the FSR lies between high sensitivity and wide measurement range, as well as between measurement speed and resolution. The core bottleneck of FSR is the order ambiguity caused by spectral overlap, high demodulation complexity, and limitations in modulation techniques. For example, high-sensitivity sensors (such as tapered fiber interferometers) are prone to spectral overlap when the spectral shift exceeds the FSR, as shown in **Figure 1**, limiting the measurement range to within a single FSR. However, it can expand the range by reducing sensitivity, but fails to meet the demands of precision measurement.

First, there is a contradiction between sensitivity and measurement range. Achieving higher sensitivity requires amplifying the impact of parameters on the spectrum, but it probably leads to spectral shifts exceeding the free spectral range, which will cause overlap. A wide measurement range requires avoiding overlap by reducing the spectral shift, which will inevitably lower the sensitivity. For instance, in high-sensitivity refractive index (RI) sensing (such as chemical concentration or biological binding detection), the sensitivity is typically quantified by the spectral shift per unit change in RI. However, if an ultra-high sensitivity is designed, a minor change in the measurand will cause a spectral shift that exceeds the FSR, leading to spectral overlap and order ambiguity. Consequently, to avoid this ambiguity, the measurement range must be severely compromised. To avoid this, the measurement range must be narrowed, which in turn affects practical needs. Second, there is a contradiction between measurement speed and resolution. By using traditional interferometers, such as the Mach-Zehnder interferometer and Sagnac interferometer, the FSR is determined by hardware parameters, which will

[1] International School for Optoelectronic Engineering, Qilu University of Technology (Shandong Academy of Sciences), Jinan, China, Laser Institute of Shandong Academy of Sciences, China-Belarus Belt and Road Joint Laboratory on Intelligent Perception in Extreme Environments
[*] Corresponding author: sdkdcd@163.com

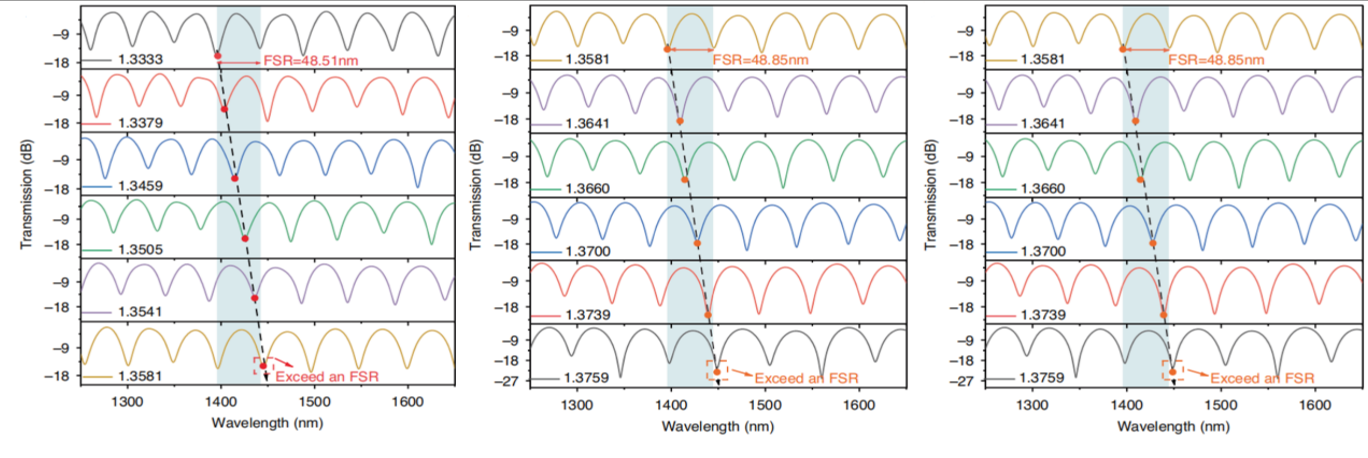

Figure 1. Spectral-overlap mechanism caused by FSR periodicity. When the wavelength shift exceeds one FSR, the shifted interference fringes re-enter adjacent periods, producing order ambiguity in peak/valley tracking and limiting the unambiguous measurement range. Adapted from Ref. [6]

make it difficult to meet the demands of high speed and high resolution. Second, there is a trade-off between the measurement dynamic range and resolution (or detection limit). In interferometric sensors, the FSR is inversely proportional to the optical path difference (OPD). A long cavity length (small FSR) yields dense interference fringes, providing ultra-high phase sensitivity and resolution; however, it severely narrows the unambiguous measurement range due to spectral overlap and demands a fine spectral scanning step, which limits the dynamic measurement speed. Conversely, a short cavity length (large F-P cavity or interferometer arm, yielding a large FSR) accommodates a wider dynamic range and faster demodulation speed, but at the expense of measurement resolution. The core issue is that traditional demodulation algorithms, such as manual peak tracking, heavily rely on local spectral features. To identify these features, the system processes a large amount of redundant information, resulting in quite long processing time.

By analyzing the contradictions arising from the influence of the FSR, it can been seen that the problem (?) is affected by factors such as spectral analysis methods and sensor structural design. Next, exploring various feasible approaches will be applied, including deep learning algorithms, the use of the Vernier effect, and sensor structural design, to clarify methods for overcoming the limitations of the FSR.

3. Methods for Breaking theFSR Limit and Their Comparison

3.1. Demodulation Algorithms

Traditional demodulation algorithms overcome FSR limitations by extracting phase, optical-path-difference, or cavity-length information from multi-wavelength/multi-channel/phase-shifting/low-coherence signals. These methods reduce reliance on a complete FSR and avoid ambiguous peak tracking when only a restricted spectral window is available. For example, Wei et al. [7] proposed a stable three-phase demodulation (STPD) architecture, as shown in **Figure 2a**. This method utilized the fixed phase difference (120°) among the three signals from a 3×3 fiber coupler for phase feedback control. By locking the operating point, the need to directly use a spectrometer was eliminated by detecting the interference spectrum (i.e., FSR shift) for calibration, as required in traditional approaches, thus achieving stable

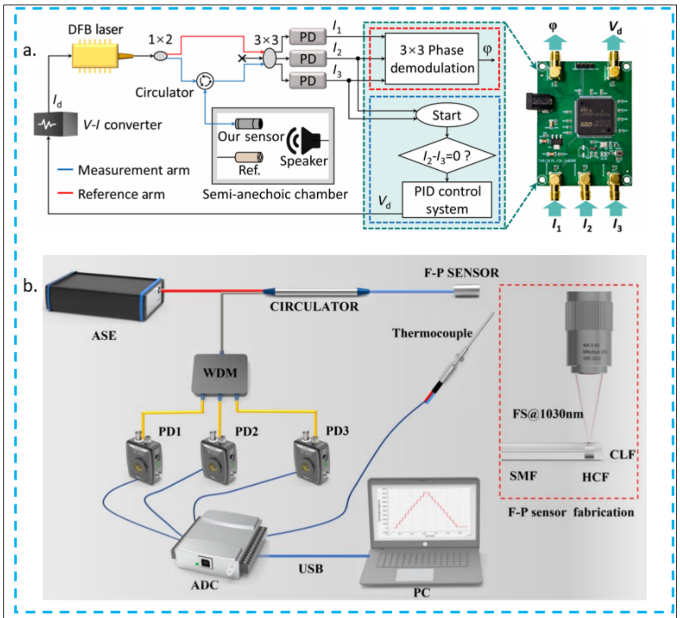

Figure 2. Demodulation schemes for extending measurable dynamic range. (a) STPD configuration using three signals with fixed 120° phase offsets from a 3 × 3 coupler to stabilize phase demodulation by feedback control. (b) Three-wavelength F-P interrogation system using fixed wavelength channels and phase compensation to recover cavity-length changes without scanning a complete FSR. Adapted from Refs. [7,8]

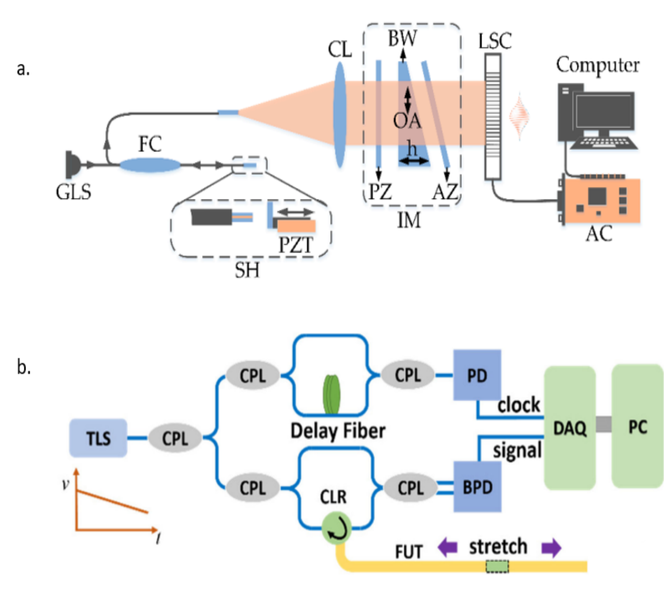

Figure 3. Low-coherence and OFDR-based demodulation schemes. (a) PLCI demodulation system using an interference-envelope extraction process to determine absolute cavity length and avoid single-period FSR ambiguity. (b) Traditional OFDR system in which phase detection and correction are used to extend distributed deformation measurements under limited spectral scanning. Adapted from Refs. [12,13]

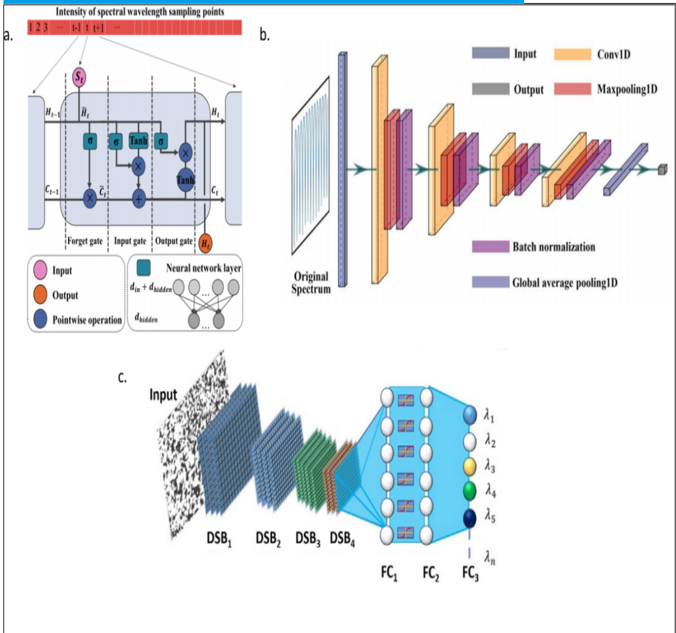

Figure 4. Representative deep-learning architectures for FSR-limited spectral demodulation. (a) LSTM memory module used to capture long-range dependencies in spectral sequences. (b) 1D-CNN architecture extracting local spectral features and peak-valley patterns. (c) DCNN model for recognizing wavelength-dependent speckle patterns over a broad dynamic range. Adapted from Refs. [14]–[16]

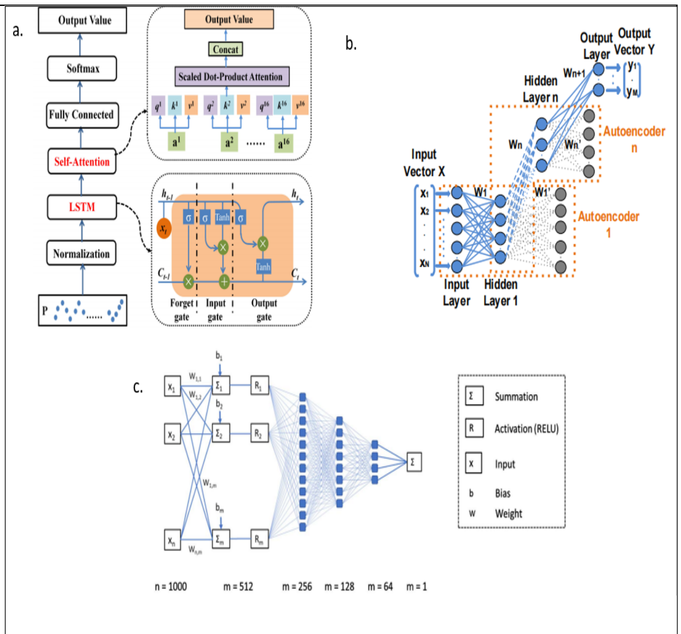

Figure 5. Neural-network models for wide-range optical sensing and multi-parameter decoupling. (a) Attention-based LSTM assigning adaptive weights to AWG-sampled spectral channels. (b) DNN with autoencoder hidden layers for simultaneous temperature and strain feature extraction. (c) MLP architecture for learning dynamic multimode interference spectra under strong noise. Adapted from Refs. [17]–[19]

phase demodulation without calibration. Guo et al. [8] employed a three-wavelength self-compensating demodulation algorithm, as shown in **Figure 2b**. Using three fixed-wavelength interference signals combined with a phase compensation algorithm, this research demodulated cavity length changes without requiring a full spectrum. By compensating for phase jumps in real time, fast and precise demodulation for any initial cavity length were achieved. Besides, this study investigated the results of breaking through the FSR limitation in dynamic measurements and making it suitable for fiber-optic F-P sensors in high-temperature, high-pressure, and high-frequency environments. Liu et al. [9] proposed a four-step phase-shifting white-light interferometry (PS-WLI) technique. The collected raw spectrum was normalized and interpolated at equal optical frequency intervals, then decomposed into four phase-shifted interference spectra with fixed phase differences. Carré algorithm was used to extract the phase. This method overcomes the traditional requirement that the spectrum must cover at least one complete FSR, thus achieving precise phase demodulation within a limited spectral range. Zhang et al. [10] proposed a linear fitting trigonometric identity transform differential cross-multiplication (LF-TIT-DCM) algorithm. This algorithm demodulates using two interference signals with a constant phase difference of Π output from a 2×2 coupler. It does not rely on spectrum acquisition or carrier frequency, thus breaking free from the physical limitation that the optical path difference must be sufficiently small in spectral demodulation methods, enabling large dynamic range demodulation. Wang et al. [11] proposed an extended FSR (EFSR) demodulation algorithm. By selecting a pair of resonant wavelengths (peaks or valleys) spaced by multiple FSRs to determine the optical path difference (OPD), the measurement errors through this averaging statistical approach were reduced, with the measurement resolution increasing exponentially with the EFSR order. Cui et al. [12] used a low-coherence interferometry combined with wavelet analysis method, as shown in **Figure 3a**. This approach no longer depends on the periodic fringes of a single wavelength, thus avoiding the FSR limitation and achieving absolute cavity length measurement. Combined with a polarization low-coherence interferometry system, the stability and repeatability of interference fringes through polarization control were enhanced. By using wavelet tools to extract the center and extreme points, the research group applied wavelet threshold denoising and complex Morlet wavelet to extract the interference fringe envelope. Based on the linear relationship between the envelope center and extreme points, the fringes of a specified order was tracked. Zhao et al. [13] proposed a phase unwrapping and phase correction algorithm based on point density distribution. By introducing phase correction to address the degradation of optical coherence caused by large strain, and using statistical filtering algorithms to process wrapped phases, high-precision distributed deformation measurement without relying on an excessively large spectral scan range was concluded.

3.2. Deep Learning Approaches

Deep learning (DL) approach provides a data-driven route to break through the limitation of FSR by learning the mapping between full spectral patterns and target measurands. Mei et al. [14,15] utilized a long short-term memory network (LSTM) storage model, which is shown in **Figure 4a**, along with the Gramian Angular Field (GAF) enhancement algorithm. A traditional Sagnac interferometer sensor measures pressure by tracking the shift of the valley wavelength. This study leverages DL to understand the mapping relationship between the full spectral intensity distribution and pressure, rather than relying on a single wavelength point. By using GAF to transform one-dimensional spectra into two-dimensional images, the model can identify deep features that persist even during spectral cyclic shifts. This method expands the measurement range from the traditional 0.34MPa to 5MPa, achieving nearly a fivefold increase in range. Additionally, to address the issues of spectral line overlap and limited measurement range caused by spectral drift exceeding the FSR in Sagnac interferometric fiber pressure sensing, a solution model centered on a one-dimensional convolutional neural network (1D-CNN) was proposed, as illustrated in **Figure 4b**, to overcome the FSR limitation on the measurement range. Gupta et al. [16] used a deep convolutional neural network (DCNN) to analyze speckle patterns generated by laser light passing through a dispersive medium, as shown in **Figure 4c**. These speckle patterns contain highly complex, disordered, but wavelength-dependent two-dimensional features. By leveraging DL to recognize speckle patterns across multiple spectral bands, this method achieves single-shot measurements over an extremely wide spectral range from 488nm to 976nm, improving the dynamic range by six orders of magnitude compared to existing technologies and completely breaking free from the physical limitations of traditional dispersion ranges. Yue et al. [17] employed an attention-based LSTM model, as shown in **Figure 5a**, using an arrayed waveguide grating (AWG) to perform multi-channel discrete sampling of the spectrum and using the sampled intensity distribution as input. The Attention-LSTM model learns the nonlinear relationship between these discrete sampling points and displacement, assigning weights to key channels, and achieves predictions independent of FSR calculations over a large displacement range of 0–830μm. Wang et al. [18] used a deep neural network (DNN) to bypass complex nonlinear equation solving, with the network structure shown in **Figure 5b**. This research

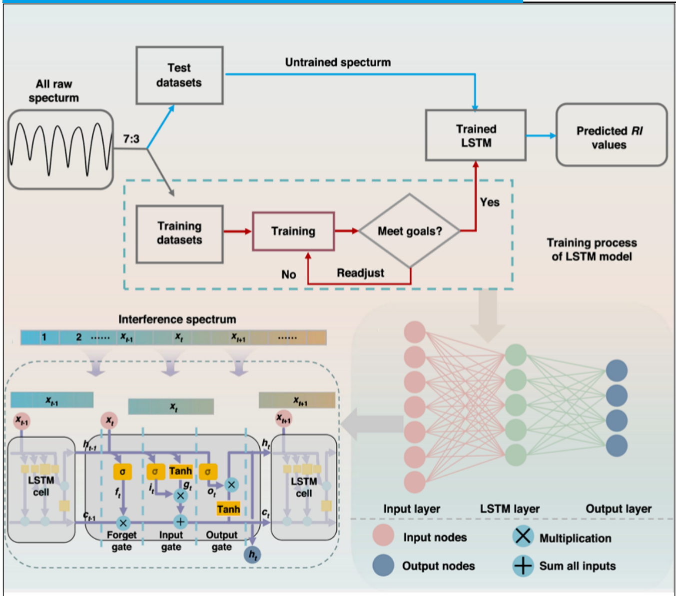

Figure 6. LSTM-based spectrum data-processing architecture for RI sensing. The model uses the full interference spectrum as sequence input and outputs predicted refractive-index values, enabling measurement beyond a single FSR without manual peak tracking. Adapted from Ref. [6]

directly extracted temperature and strain features from the overall shape of the bimodal spectrum, solving the problem of traditional methods being unable to accurately demodulate when spectral features overlap or the signal-to-noise ratio is low. Nguyen et al. [19] used a multilayer perceptron (MLP) DNN, as shown in **Figure 5c**, treating the entire dynamic interference spectrum as a statistical feature set and using DL learn the evolution patterns of spectral features under changes in the measured physical quantity. This method maintains a large measurement range even in strong environments, accurately predicting even when spectral phase shifts undergo multiple cyclic overlaps. Hu et al. [6] used a LSTM, as shown in **Figure 6**, to address the contradiction between high sensitivity and FSR in Mach-Zehnder interferometer (MZI)-type refractive index (RI) sensors. By leveraging the excellent gating mechanism of LSTM to process spectral sequence data with long-term dependencies, they directly establish a mapping relationship between the full interference spectrum and the refractive index value, eliminating the need for complex traditional spectral signal analysis. This expands the measurement range from one free spectral range to three free spectral ranges.

Overall, the reviewed DL-based fiber optic sensing signal demodulation and multi-physical-quantity decoupling techniques represent a promising development direction. In traditional weak grating arrays and superstructure FBG(?) sensing networks, the reflection peaks of adjacent gratings are prone to spectral overlap, and the strain measurement range is strictly limited by the FSR of the FBG. Conventional peak-tracking and cross-correlation algorithms can neither handle aliased spectra nor resolve wavenumber tracking errors caused by peak jumps, and the dynamic range is confined to within 2000με. By treating spectral demodulation as a wavenumber-tracking task on time-series sequences and using an evolutionary attention mechanism to enhance weak spectral feature extraction, DL methods can address peak jumps and spectral overlap. Reported experiments have achieved an ultra-large strain measurement range of 16000με, eight times that of traditional methods, with a demodulation accuracy of ±5με. Compared with traditional demodulation algorithms, DL can reduce dependence on phase periodicity and manual peak tracking, exhibits strong robustness to noise, and can handle long-term FSR drift dependencies. For network architecture selection, 1D-CNNs are effective for extracting local spectral shape features and relative peak-valley changes; LSTM/GRU models are suitable for long-sequence spectral data and dispersed spectral feature distributions; and dimensionality-increase approaches such as Gramian Angular Fields and Markov transition fields convert 1D spectra into 2D images so that 2D-CNNs can exploit spatial feature extraction. Therefore, for many fiber optic sensing and optical measurement scenarios, DL is a practical and universal back-end strategy for mitigating FSR-induced demodulation ambiguity without modifying existing hardware or optical structures.

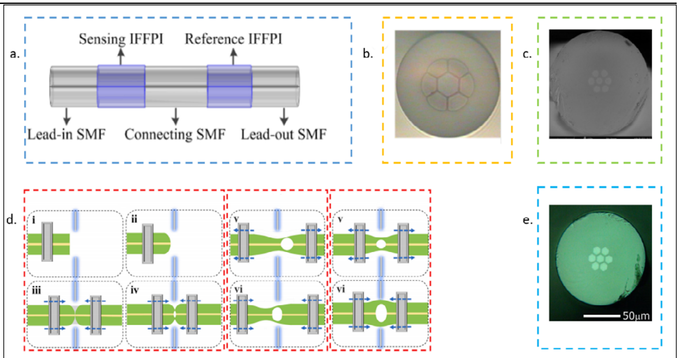

Figure 7. Structural designs for Vernier-effect FSR extension. (a) Cascaded intrinsic fiber Fabry-Perot interferometers in which slightly mismatched cavity lengths generate a large-period Vernier envelope. (b) HC-PCF cross-section used to form compact F-P cavities. (c) Strongly coupled multicore-fiber cross-section for enhanced bending response. (d) Arc-discharge tuning process for a bubble microcavity, enabling fine FSR matching. (e) Seven-core-fiber cross-section used to construct cascaded or parallel Vernier configurations. Adapted from Refs. [20]–[23]

3.3. Structural Design

Structural design provides a direct physical route to overcome the limitation of FSR, especially through the optical Vernier effect and geometry-controlled resonator tuning. By connecting two interferometers with very close FSRs (one as the sensing unit and the other as the reference unit) in series or parallel, their superimposed spectrum generates a low-frequency envelope. The FSR of this envelope is much larger than that of a single interferometer, and tracking the drift of the envelope can significantly enhance sensitivity. Zhang et al. [20] used hollow-core photonic crystal fiber (HC-PCF) to form cascaded intrinsic fiber Fabry-Perot interferometers (IFFPIs) as shown in **Figure 7a** to produce a Vernier effect, with the fiber cross-section shown in **Figure 7b**. By designing two IFFPIs with a slight cavity length difference, their superimposed reflection spectra produce a Vernier envelope with large FSR characteristics, utilizing the periodicity of the Vernier envelope to track external changes, thereby greatly improving sensitivity. Ou et al. [21] cascaded two sections of strongly coupled seven-core fiber with slight length differences, as shown in the cross-section in **Figure 7c**. One section served as the sensor, and the other as the reference. Due to the different FSRs of the two structures, the bending sensitivity was amplified approximately 19 times through the Vernier effect. Liu et al. [22] proposed an iterative arc dissolution tuning method to address the difficulty of precise FSR matching in Vernier effect sensors. By applying multiple weak arc discharges to a bubble microcavity and monitoring the spectrum in real time to adjust the bubble cavity length, as shown in the fabrication process in **Figure 7d**, this method allows low-cost, high-success-rate, fine-tuning of the FSR until a perfect Vernier envelope is achieved. Cuando-Espitia et al. [23] used two sections of highly coupled seven-core fiber with different lengths, as shown in the cross-section in **Figure 7e**, as basic units to construct four different cascaded or parallel configurations. Through the Vernier effect, the temperature sensitivity was enhanced by 10-12 times. Zhou et al. [24] introduced the harmonic Vernier effect (HVE) to fabricate sensors as shown in **Figure 8a**. By making the optical path length (OPL) of one interferometer an integer multiple (harmonic order i) of the other, this achieves not only a higher sensitivity amplification factor than the traditional Vernier effect, but also significantly relaxes the OPL matching error constraints during fabrication. Zhou et al. [25] proposed an enhanced Vernier effect, with the system schematic shown in **Figure 8b**. By cascading fiber loop interferometers, the effective length differences of three interference paths were designed, so that when the temperature changes, one FSR decreases while the other increases simultaneously. This variation greatly magnifies the difference between the two FSRs, doubling the sensitivity improvement. Lee et al. [26] employed refractive index-selective liquid filling in hollow-core fiber (HCF) with a liquid refractive index slightly lower than the silica cladding, as shown in **Figure 9**, to precisely control the effective refractive index difference of the modes. By matching the refractive index of the liquid with the length of the interference section, the FSR exceeds the entire measurement window, collapsing the originally dense interference fringes into a single-wavelength notch, achieving an ultra-wide FSR. Sharma et al. [27] placed two uncoated standard communication fibers at a very small angle to cross each other,

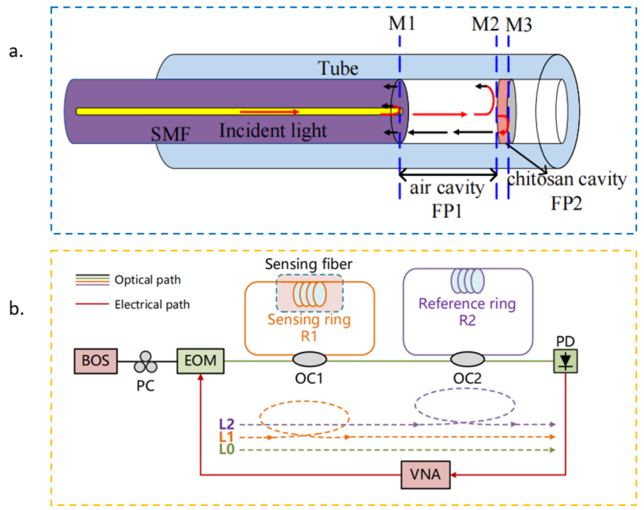

Figure 8. Advanced Vernier configurations for sensitivity amplification. (a) Harmonic Vernier FPI sensor in which the optical path length of one interferometer is set to a harmonic multiple of the other to increase the amplification factor and relax fabrication tolerances. (b) Enhanced Vernier temperature-sensing system based on cascaded fiber loop interferometers, where opposite FSR variations increase envelope-shift sensitivity. Adapted from Refs. [24,25]

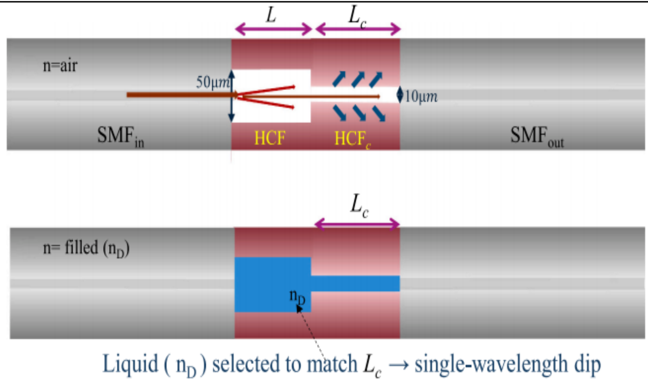

Figure 9. Refractive-index-selected liquid-core S-FMZI for ultrabroad FSR control. Filling the air core with a liquid whose refractive index is matched to the coupling length reduces modal effective-index difference and collapses dense fringes into a single-wavelength dip. Adapted from Ref. [26]

as shown in **Figure 10a**. The distance between the fiber surfaces near the crossing point is extremely close, generating coupling through the evanescent field. As the rotation angle increases, the contact area disappears, shortening the effective length of the coupling region, which reduces the axial size of the resonator and increases the FSR, thereby achieving millimeter-scale control of the physical length of the resonator and fine-tuning the FSR at the picometer scale. Vassiliev et al. [28] pre-bent an optical fiber into a certain curvature and brought it into contact with another straight fiber, as shown in **Figure 10b**. The contour of the bent fiber determines the coupling strength and coupling region between it and the straight fiber. By changing the bending radius R of the bent fiber, the axial length of the coupling region can be altered. When R is reduced from the centimeter scale to the millimeter scale, the coupling region shortens from the millimeter scale to the hundred-micrometer scale. This coupling region defines a SNAP microresonator, whose axial dimension determines the FSR. Thus, the FSR can be tuned from the picometer scale to the tens of picometer scale.

3.4. Material Selection and Properties

Material selection and property engineering offer another route for expanding or effectively overcoming FSR limitations by changing the effective refractive index, propagation path, resonance condition, or gain bandwidth of photonic devices. Ding et al. [29] designed cascaded racetrack-type microring resonators (MRRs) on a lithium niobate on insulator (LNOI) platform, as shown in **Figure 11a**, utilizing the thermo-optic (TO) effect for active tuning. Through wavelength shifting, the tuning range is sufficient to cover the entire FSR, thereby fully compensating for resonant frequency mismatches caused by fabrication errors or temperature fluctuations, and maintaining stable filter performance. Aliqab et al. [30] combined phase-change material (GST) and graphene in a multilayer structure, as shown in **Figure 11b**. GST exists in both amorphous and crystalline states with a significant refractive index difference, and its state can be easily altered by external stimuli, allowing substantial adjustment of the effective refractive index. This enables fine spectral tuning

Table 1. Comparison of different technical routes for breaking through the FSR limitation.

Technical Route	Core Operating Principle	Representative Works	Key Advantages	Major Limitations / Challenges	Typical Applications
Demodulation Algorithms	Phase/OPD tracking from multi-wavelength or phase-shifting signals; avoids full-spectrum scanning.	Ref. [7], [8], [11]	• Low hardware cost • Fast processing speed • Mathematically rigorous	• Limited dynamic range expansion • Sensitive to noise-induced phase jumps	Dynamic acoustic/vibration sensing; high-precision F-P sensing
Deep Learning Approaches	Data-driven mapping between full-spectrum profiles and target measurands; extracts shift-invariant features.	Ref. [6], [14], [16]	• High noise tolerance • Bypasses complex physical equations • Resolves severe spectral overlaps	• Requires massive training datasets • Lack of physical interpretability ("black box")	Multi-parameter decoupling; extreme-environment sensing; speckle spectrometers
Structural Design	Envelope tracking via mismatched cascaded cavities (Vernier effect) or physical tuning of resonators.	Ref. [20], [24], [26]	• Enormous passive sensitivity amplification • No active power consumption	• High fabrication complexity • Strict tolerance for cavity length matching	Ultra-sensitive temperature, strain, and bending sensors
Material Selection & Properties	Dynamic tuning of effective refractive index (n_{eff}) or material dispersion using active external stimuli.	Ref. [29], [31], [33]	• Active, fast, and continuous tuning • Reconfigurable dispersion • Mode-hopping-free	• Complex integration (nanostructures) • High active power consumption (thermal) • Long-term material degradation	On-chip tunable filters; microresonators; reconfigurable nonlinear photonics

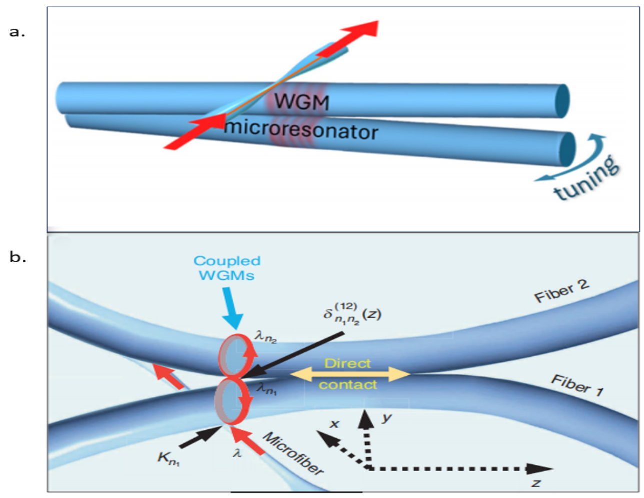

Figure 10. Geometry-tuned WGM/SNAP microresonators for FSR adjustment. (a) WGM microresonator induced at the intersection of straight optical fibers, where the crossing angle changes the effective coupling length and resonator size. (b) Side-coupled bent-fiber configuration in which the bending radius controls the coupling region and thereby tunes the SNAP microresonator FSR. Adapted from Refs. [27,28]

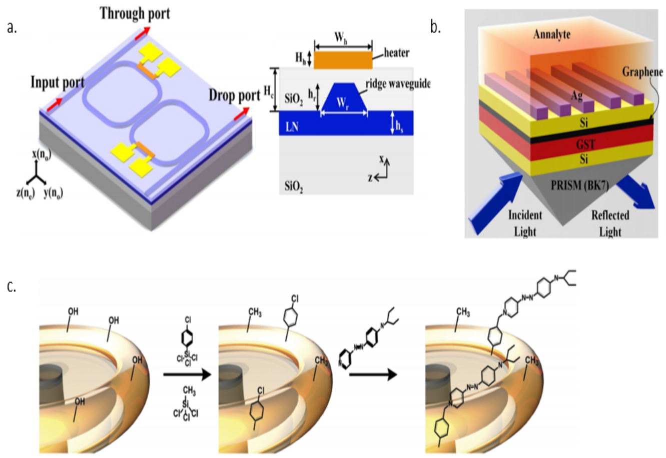

Figure 11. Material-enabled tuning mechanisms for broad spectral control. (a) LNOI tunable optical filter with integrated heaters, where the thermo-optic effect shifts racetrack microring resonances. (b) Multilayer SPR biosensor combining phase-change material and graphene to tune effective refractive index. (c) Azobenzene-monolayer functionalization scheme, where photoisomerization changes the microresonator surface refractive index. Adapted from Refs. [29]–[31]

and adjustment of resonant peaks over a wide wavelength range, overcoming the narrow refractive index tuning range of single materials. Kovach et al. [31] functionalized the surface of a silica microcavity with a monolayer of azobenzene derivative to break through the tuning range limitation. The process flow for forming a photoresponsive monolayer is shown in **Figure 11c**. By utilizing light-induced cis-trans isomerization to change the refractive index of the molecular layer, a 60% FSR resonant frequency tuning range was achieved. This all-optical control mechanism avoids the difficulty of achieving large-scale wavelength shifts in large devices using traditional electrical tuning methods. Hong et al. [32] employed a Fano resonator structure combined with a graphene nanoheater, as shown in **Figure 12**. Due to the asymmetric line shape of Fano resonance, it has a steeper slope in the wavelength range from minimum to maximum transmittance compared to traditional Lorentzian resonance. This characteristic reduces the required wavelength shift for state switching, achieving tuning with only 1mW of power, greatly improving switching efficiency within a limited FSR. Chen et al. [33] combined the ultra-broadband Raman gain of tellurite fiber with the active gain of erbium-doped fiber (EDF). Crucially, unlike traditional lasers that suffer from discrete longitudinal mode hopping governed by the cavity's FSR, random fiber lasers (RFLs) lack a fixed physical cavity and are inherently FSR-free. By combining the complementary gains of tellurite and erbium-doped fibers, this approach achieves an ultra-wide, continuous, and mode-hopping-free tuning range of 160 nm, completely bypassing the spectral limitations imposed by traditional cavity resonance. Traditional random lasers are limited to a single medium. By introducing EDF to fill the gain gap of tellurite at 1560-1590 nm, a tunable RFL (random fiber laser) scheme is realized, as shown in **Figure 13a**, achieving ultra-wide continuous tuning covering the entire S, C, and L bands (1480-1640nm) with a 160nm range, breaking spectral limitations in terms of bandwidth. Xia et al. [34] utilized the photosensitivity of chalcogenide glass (GeSbS) to non-volatilely imprint or erase Bragg gratings within the cavity through standing wave patterns generated by backscattering. The detailed structure of the GeSbS microresonator is shown in **Figure 13b**. This mechanism allows dynamic synthesis of dispersion curves. By inducing strong mode splitting, the frequency of individual transverse modes can be precisely

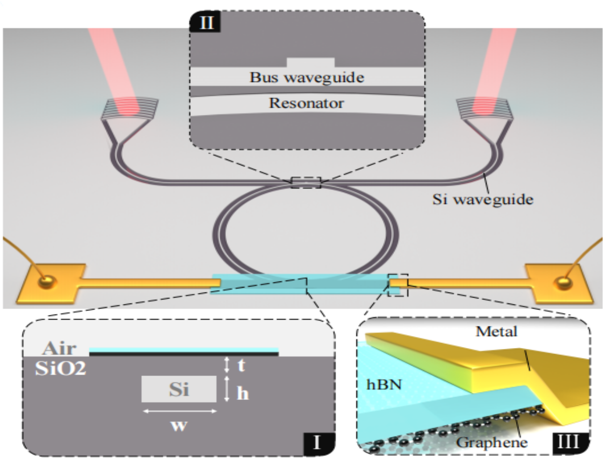

Figure 12. Fano resonator with a graphene nanoheater. The asymmetric Fano line shape enables switching over a small wavelength shift, while localized graphene heating provides low-power resonance tuning within the available FSR. Adapted from Ref. [32]

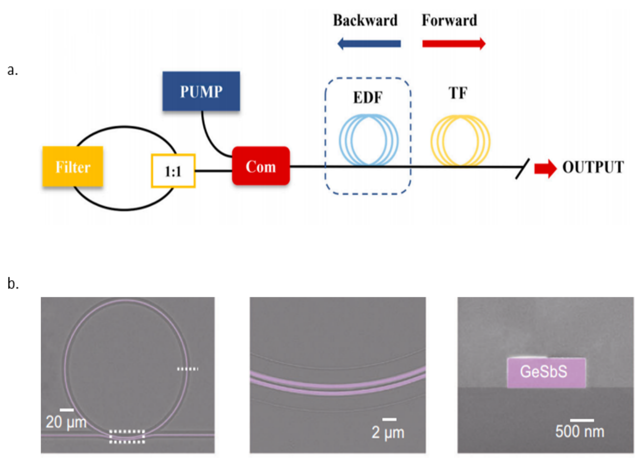

Figure 13. Broadband material and nonlinear-photonic schemes. (a) Tunable random fiber laser combining tellurite fiber and erbium-doped fiber to cover the S, C, and L bands through complementary gain. (b) GeSbS chalcogenide microresonator structure enabling non-volatile, photosensitive grating imprinting and reconfigurable dispersion control. Adapted from Refs. [33,34]

shifted, breaking the matching limitation of FSR on nonlinear processes without changing the resonator size.

4. Summary and Outlook

The limitation of the FSR is a key bottleneck constraining the performance of optical interference sensing and filtering. As reviewed above, current strategies can be grouped into four complementary routes: demodulation algorithms, DL-assisted demodulation, structural design, and material-property engineering. Through the integration of multidisciplinary fields such as artificial intelligence (AI) and multi-wavelength interference, various effective techniques have emerged to overcome FSR limitations [35]–[39]. Among these, AI-based signal processing and spectral-feature extraction enable more intelligent sensing systems [6],[14]–[19],[41]; material dispersion control and emerging tunable materials support higher Q-values and broader tuning ranges [29]–[34],[40]–[43]; structural expansion methods based on multi-wavelength interference and the Vernier effect utilize cavity matching, cascaded structures, and envelope tracking to produce ultrabroad or high-sensitivity responses [20]–[28],[45]; and microresonator tuning techniques provide continuous adjustability and high uniformity of FSR [27],[28],[43]. However, these techniques still face challenges such as trade-offs between sensitivity and dynamic range, system complexity and high cost, insufficient environmental stability and repeatability, and a lack of standardization. In the future, integrating artificial intelligence with physical expansion techniques, exploring new materials and structures to enhance capabilities, and advancing system integration and networking to build higher-channel sensing systems will be key directions for breaking through FSR limitations in optical sensing, thereby moving toward higher performance, greater intelligence, and broader applications.

Author Contributions

H.M. conceived the review topic and designed the overall framework of the manuscript; R.L. and F.L. conducted the literature search and collected relevant references; M.G. and Z.Z. analyzed, summarized, and compared the reported methods for breaking through the free spectral range limitation; H.W. and Q.G. assisted in organizing the manuscript content, preparing figures, and revising the manuscript; D.C. supervised the entire review process, provided funding support, and revised and finalized the manuscript. All authors have read and approved the final manuscript.

Funding

Shandong Provincial Natural Science Foundation (ZR2022QF083); Taishan Scholar Youth Expert Program (tsqn202306254); Talent Introduction Program of Qilu University of Technology (2023RCKY033); Jinan Higher Education Innovation Project (2023GXRC062): Optical Fiber Sensing Technology for Oil and Gas Well Monitoring (Project Funding: 300,000 RMB, Implementation Period: 2024–2026)

Conflicts of Interest

The authors declare that the research was conducted in the absence of any commercial or financial relationships that could be construed as a potential conflict of interest.

References

[1] M. H. Yang, Y. X. Ye, Q. L. Nie, Z. X. Liu, M. E. Cheng, D. L. Guo, "Review on Research Progress of Optical Fiber Sensing Technology in Energy Storage Battery Performance Monitoring." *Laser Optoelectron. Prog.* **2023**, *11*, 60, 1106006.

[2] J. J. Tian, Y. Z. Jiao, S. B. Ji, X. L. Dong, Y. Yao, "Cascaded-Cavity Fabry–Perot Interferometer for Simultaneous Measurement of Temperature and Strain with Cross-Sensitivity Compensation." *Opt. Commun.* **2018**, 412, 121–126.

[3] Y. Yang, B. Xu, Y. M. Liu, P. Li, D. N. Wang, C. L. Zhao, "Sensitivity-Enhanced Temperature Sensor with Fiber Optic Fabry–Perot Interferometer Based on Vernier Effect." *Acta Phys. Sin.* **2017**, *9*, 66, 094205.

[4] H. Li, Q. C. Zhao, S. D. Jiang, J. S. Ni, C. Wang, "FP Cavity and FBG Cascaded Optical Fiber Temperature and Pressure Sensor." *Chin. Opt. Lett.* **2019**, *4*, 17, 040603.

[5] J. Yi, "Sapphire Fabry–Perot Pressure Sensor at High Temperature." *IEEE Sens. J.* **2021**, *2*, 21, 1596–1602.

[6] J. L. Hu, S. Zhang, M. Y. Cai, M. J. Ma, S. G. Li, H. L. Chen, S. G. Yang, "LSTM-Assisted Optical Fiber Interferometric Sensing: Breaking the Limitation of Free Spectral Range." *Light Sci. Appl.* **2025**, *1*, 14, 392.

[7] X. Y. Wei, J. D. Du, J. F. Zhou, X. L. Deng, Z. R. Yi, L. Shao, W. M. Zhang, "Multiresonant Fiber Acoustic Sensors with Stabilized Triple-Phase Demodulation for Large Dynamic Ranges." *Adv. Devices Instrum.* **2025**, 6, 0081.

[8] M. C. Guo, Q. Zhang, H. T. Zhu, R. Liang, Y. Q. Zheng, X. Zhu, E. B. Wang, Z. Y. Li, C. Y. Xue, Z. Y. Hai, "Performance Study of F-P Pressure Sensor Based on Three-Wavelength Demodulation: High-Temperature, High-Pressure, and High-Dynamic Measurements." *Sensors* **2024**, *16*, 24, 5313.

[9] Q. Liu, L. B. Gao, D. D. Lin, J. Z. Shi, D. Zhu, Y. P. Wang, "Phase Interrogation of Fiber-Optic Interferometric Acoustic/Vibration Sensors in Restricted Spectral Ranges." *IEEE Sens. J.* **2024**, *21*, 24, 34576–34583.

[10] W. J. Zhang, P. Lu, Z. Y. Qu, J. S. Zhang, Q. Wu, D. M. Liu, "Large-Dynamic-Range and High-Stability Phase Demodulation Technology for Fiber-Optic Michelson Interferometric Sensors." *Sensors* **2022**, *7*, 22, 2488.

[11] S. Wang, L. Mohanty, Y. Yang, "An Accurate Demodulation Method for Fiber-Optic Interferometric Sensors Based on the Expanded Free Spectral Range." *IEEE Sens. J.* **2023**, *3*, 23, 2241–2248.

[12] J. Cui, Y. Niu, H. Dang, K. Feng, X. Sun, J. Tan, "Demodulation Method of F-P Sensor Based on Wavelet Transform and Polarization Low Coherence Interferometry." *Sensors* **2020**, *15*, 20, 4249.

[13] S. Zhao, J. Cui, Z. Wu, Z. Wang, J. Tan, "Distributed Fiber Deformation Measurement by High-Accuracy Phase Detection in OFDR Scheme." *J. Lightwave Technol.* **2021**, *12*, 39, 4101–4108.

[14] Y. Mei, S. Zhang, Z. Cao, T. Xia, X. Yi, Z. Liu, "Deep Learning Assisted Pressure Sensing Based on Sagnac Interferometry Realized by Side-Hole Fiber." *J. Lightwave Technol.* **2023**, *2*, 41, 784–793.

[15] Y. Mei, S. Zhang, Z. Cao, T. Xia, X. Yi, Z. Liu, "High Accuracy Pressure Sensing with Sagnac Interferometry Based on Deep Learning Approach." *Proc. IEEE 24th Int. Workshop Multimed. Signal Process. (MMSP)* **2022**, 1–5.

[16] R. K. Gupta, G. D. Bruce, S. J. Powis, K. Dholakia, "Deep Learning Enabled Laser Speckle Wavemeter with a High Dynamic Range." *Laser Photonics Rev.* **2020**, *9*, 14, 2000120.

[17] Z. Yue, D. Zheng, X. Zou, C. Xie, Y. Peng, "Large Dynamic Range Interrogation Technique for Fiber-Optic Interferometric Sensor Based on AWG and Deep Learning Algorithm." *IEEE Sens. J.* **2024**, *1*, 24, 278–286.

[18] B. Wang, L. Wang, N. Guo, Z. Zhao, C. Yu, C. Lu, "Deep Neural Networks Assisted BOTDA for Simultaneous Temperature and Strain Measurement with Enhanced Accuracy." *Opt. Express* **2019**, *3*, 27, 2530–2543.

[19] L. V. Nguyen, C. C. Nguyen, G. Carneiro, H. Ebendorff-Heidepriem, S. C. Warren-Smith, "Sensing in the Presence of Strong Noise by Deep Learning of Dynamic Multimode Fiber Interference." *Photonics Res.* **2021**, *4*, 9, B109–B118.

[20] P. Zhang, M. Tang, F. Gao, B. Zhu, S. Fu, J. Ouyang, P. P. Shum, D. Liu, "Cascaded Fiber-Optic Fabry–Perot Interferometers with Vernier Effect for Highly Sensitive Measurement of Axial Strain and Magnetic Field." *Opt. Express* **2014**, *16*, 22, 19581–19588.

[21] J. Ou, H. W. Deng, C. Wu, J. Li, B. O. Guan, "Cascaded Multicore Fiber Interferometers for Enhanced Bending Sensing Based on the Vernier Effect." *Opt. Express* **2024**, *8*, 32, 14143–14153.

[22] C. Liu, J. Wang, J. Lv, X. Song, W. Liu, Q. Liu, R. Li, L. Li, Z. Yi, P. K. Chu, "Economical and Easily Implemented Vernier Effect Bubble Microcavity FPI for Strain Sensing with Extreme Low-Temperature Cross-Sensitivity." *Infrared Phys. Technol.* **2025**, 150, 105939.

[23] N. Cuando-Espitia, M. A. Fuentes-Fuentes, A. Velázquez-Benítez, R. Amezcua, J. Hernández-Cordero, D. A. May-Arrioja, "Vernier Effect Using In-Line Highly Coupled Multicore Fibers." *Sci. Rep.* **2021**, *1*, 11, 18383.

[24] C. Zhou, Y. Song, Q. Zhou, J. Tian, Y. Yao, "Ultra-High-Sensitivity Humidity Fiber Sensor Based on Harmonic Vernier Effect in Cascaded FPI." *Sensors* **2022**, *13*, 22, 4816.

[25] J. Zhou, Y. Zhi, J. Zhang, J. Yao, J. Zhang, J. Zhang, "Enhanced Vernier Effect in Cascaded Fiber Loop Interferometers for Improving Temperature Sensitivity." *Sensors* **2025**, *1*, 25, 38.

[26] C. L. Lee, Y. H. Lu, W. J. Chen, Y. C. Hsia, C. H. Shih, W. H. Hsieh, "Ultrabroadband Single-Wavelength Dip in a High-Sensitivity Fiber Mach–Zehnder Interferometer Using a Refractive-Index-Selected Liquid Core." *Sens. Actuators A Phys.* **2026**, 398, 117355.

[27] I. Sharma, M. Sumetsky, "Widely FSR Tunable High Q-Factor Microresonators Formed at the Intersection of Straight Optical Fibers." *Optica* **2025**, *6*, 12, 890–893.

[28] V. Vassiliev, M. Sumetsky, "High Q-Factor Reconfigurable Microresonators Induced in Side-Coupled Optical Fibres." *Light Sci. Appl.* **2023**, *1*, 12, 197.

[29] Y. Ding, S. Tao, X. Wang, C. Shang, A. Pan, C. Zeng, J. Xia, "Thermo-Optic Tunable Optical Filters with GHz-Bandwidth and Flat-Top Passband on Thin Film Lithium Niobate Platform." *Opt. Express* **2022**, *12*, 30, 22135–

22142.
[30] K. Aliqab, K. Dave, V. Sorathiya, M. Alsharari, A. Armghan, "Numerical Analysis of Phase Change Material and Graphene-Based Tunable Refractive Index Sensor for Infrared Frequency Spectrum." *Sci. Rep.* **2023**, *1*, 13, 7653.
[31] A. Kovach, J. He, P. J. G. Saris, D. Chen, A. M. Armani, "Optically Tunable Microresonator Using an Azobenzene Monolayer." *AIP Adv.* **2020**, *4*, 10, 045117.
[32] Q. Hong, J. Jiang, S. Zhou, G. Xia, P. Xu, M. Zhu, W. Xu, J. Zhang, Z. Zhu, "Silicon-Based On-Chip Tunable High-Q-Factor and Low-Power Fano Resonators with Graphene Nanoheaters." *Nanomaterials* **2023**, *10*, 13, 1636.
[33] L. Chen, Y. Li, H. Liang, H. Wu, "A Theoretical Investigation of an Ultrawide S-, C- and L-Band-Tunable Random Fiber Laser Based on the Combination of Tellurite Fiber and Erbium-Doped Fiber." *Photonics* **2024**, *3*, 11, 247.
[34] D. Xia, L. Luo, L. Wang, X. Zhao, Z. Yang, J. Wu, Q. F. Yang, Z. Li, B. Zhang, "Reconfigurable Chalcogenide Integrated Nonlinear Photonics." *Nat. Commun.* **2025**, *1*, 16, 10133.
[35] C. Sun, C. Zhong, M. Wei, H. Ma, Y. Luo, Z. Chen, R. Tang, J. Jian, H. Lin, L. Li, "Free-Spectral-Range-Free Filters with Ultrawide Tunability across the S + C + L Band." *Photonics Res.* **2021**, *6*, 9, 1013–1018.
[36] C. Feng, X. Wang, B. Miao, Z. Gu, J. Li, "Real-Time Free Spectral Range Measurement Based on a Correlated Resonance-Tracking Technology." *Opt. Express* **2023**, *19*, 31, 30604–30614.
[37] M. Xiang, Y. M. Cai, Y. M. Wu, J. Y. Yang, Y. L. Wang, "Experimental Study of the Free Spectral Range (FSR) in FPI with a Small Plate Gap." *Opt. Express* **2003**, *23*, 11, 3147–3152.
[38] Y. Chen, C. Zhang, Y. K. Zhao, L. Lu, "Measurement of Laser Free Spectral Range Based on Three-Longitudinal Mode Laser Self-Mixing Sensing System." *Chin. J. Quantum Electron.* **2020**, *6*, 37, 669.
[39] H. Xu, Y. Qin, G. Hu, H. K. Tsang, "Integrated Single-Resonator Spectrometer beyond the Free-Spectral-Range Limit." *ACS Photonics* **2023**, *3*, 10, 654–666.
[40] H. Jeong, K. Oh, "Enhancement of Free Spectral Range of the Resonance Peaks in a Long-Period Fiber Grating by Controlling Material Dispersion of Cladding Modes." *Opt. Commun.* **2001**, *1–4*, 199, 103–110.
[41] A. Ahamed, H. Myat, A. Rawat, L. N. McPhillips, M. S. Islam, "AI-Augmented Photon-Trapping Spectrometer-on-a-Chip on Silicon Platform with Extended Near-Infrared Sensitivity." *Adv. Photonics* **2026**, *1*, 8, 016008.
[42] P. He, J. Li, C. Li, N. Li, B. Han, R. Shi, R. Qi, J. Du, P. Yu, P. Gao, "Strongly Confined Mid-Infrared to Terahertz Phonon Polaritons in Ultrathin $SrTiO_3$." *Sci. Adv.* **2025**, *47*, 11, eady7316.
[43] M. Crespo-Ballesteros, M. Sumetsky, "Ultra-Precise, Sub-Picometer Tunable Free Spectral Range in a Parabolic Microresonator Induced by Optical Fiber Bending." *Opt. Lett.* **2024**, *15*, 49, 4354–4357.
[44] C. H. Lee, X. Ren, X. Su, W. Lee, Z. Jiang, Y. Yu, H. Zhou, Y. Zuo, S. Ou, R. Kopparapu, A. T. Heiniger, M. Tur, A. E. Willner, Z. Chen, M. Yu, "Suspended Thin-Film Lithium Niobate Modulator for Broadband Mid-Infrared Light Modulation and Frequency Comb Generation." *arXiv* **2026**, arXiv:2601.17385.
[45] Y. Liu, H. Xu, K. Zhu, Y. Yao, Y. Suo, L. Zhang, "Erbium-Doped Tunable Fiber Laser Based on a Vernier Effect Filter." *Photonics* **2024**, *10*, 11, 979.